Central collisions produced by relativistic heavy ions in nuclear emulsion

H. H. Heckman, H. J. Crawford, D. E. Greiner, P. J. Lindstrom, and Lance W. Wilson
Lawrence Berkeley Laboratory and Space Sciences Laboratory, University of California, Berkeley, California 94720
(Received 22 August 1977)

We have performed an experimental study of the angular and momentum distributions of fragments emitted from central collisions between emulsion nuclei (AgBr) and heavy-ion projectiles ^{4}He, ^{16}O, and ^{40}Ar at beam rigidity 5.72 GV. Central collisions are here defined as interactions that exhibit an absence of projectile fragmentation, i.e., no beam-velocity fragments are produced within 5° of the incident beam direction. Production angles have been measured for all fragments having a restricted gain density $g \geq 2g_{\min}$ corresponding to protons of $E \leq 250$ MeV. Both range and angle measurements have been made for fragment ranges ≤ 4 mm, corresponding to protons of $E \leq 31$ MeV. The data are analyzed in terms of a modified Maxwell-Boltzmann distribution from which we obtain estimates of the longitudinal velocity $\beta_{\parallel}$ and the characteristic spectral volocity β_0 of the particle-emitting systems. We find that no unique Maxwellian distribution can account for the observed fragment distributions. The angular distributions do not display statistically significant structure attributable to collective phenomena.

[NUCLEAR REACTIONS AgBr(^{4}He,x), $E=2.1$ GeV/A; AgBr(^{16}O,x), $E=2.1$ GeV/A; and AgBr(^{40}Ar,x), $E=1.8$ GeV/A; measured fragment multiplicities; range and angular distributions for ranges ≤4 mm ($E_{\text{proton}} \leq 31$ MeV); angular distribution for $E_{\text{proton}} \leq 250$ MeV. Nonperipheral collisions, Maxwell-Boltzmann parametrization.]

I. INTRODUCTION

The characteristic features of the interactions between nuclei at relativistic energies, from a geometrical concept, depend sensitively on the impact parameter of the collision. In particular, if R_1 and R_2 are the radii of the target and projectile nuclei, respectively, the limiting values of the impact parameter b give rise to the concepts of peripheral collisions, i.e., $b \approx R_1 + R_2$, and of central collisions, where $0 \lesssim b \lesssim |R_1 - R_2|$. Peripheral collisions characteristically exhibit the emission of fragments of the projectile in a narrow forward cone, whose angular width is determined by the intrinsic Fermi-momentum distributions of the nucleons within the fragmenting nucleus. Figure 1 is a photomicrograph of an ^{40}Ar interaction observed in this experiment that shows typical features of a peripheral collision. In contrast, central collisions give rise to a large range of complex phenomena that can result in the catastrophic destruction of the interacting nuclei. The occurence of such an event is shown in Fig. 2. Here, the interaction between the ^{40}Ar projectile and target nucleus involves high levels of excitation and the emission of a large number of secondary fragments, predominantly nucleons and light fragments. Because central collisions at high energies subject nuclear matter to physical conditions heretofore unavailable in the laboratory, there is

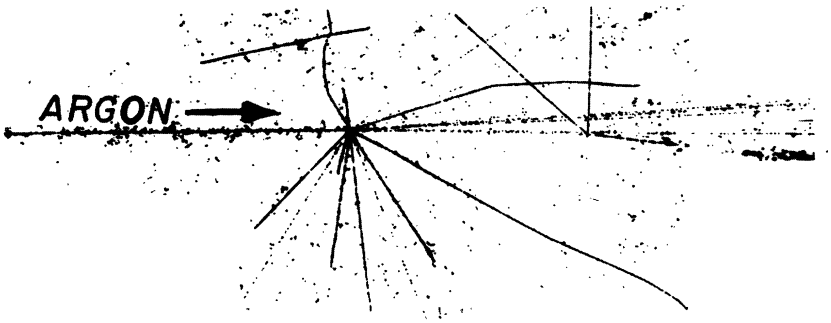

FIG. 1. An interaction of an ^{40}Ar projectile, $E=1.8$ GeV/A, observed in Ilford G.5 emulsion that shows the characteristic of projectile and target (AgBr) fragmentation. The forward cone of (5) He fragments, one of which produces a secondary interaction, indicates a peripheral collision has taken place. A π^- meson produced in the interaction is brought to rest and forms a three-prong star (above the point of interaction).

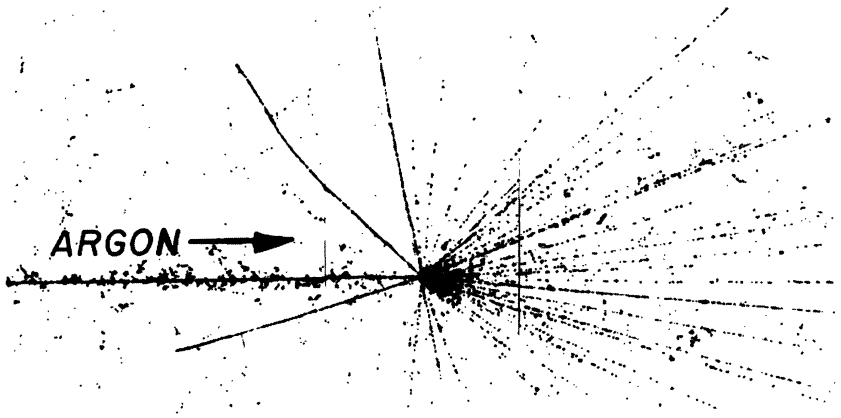

FIG. 2. An interaction of an ^{40}Ar projectile, $E=1.8$ GeV/A, with a heavy emulsion nucleus that leads to catastrophic destruction of the projectile and target nuclei. This example of a central collision has 63 fragment tracks—the largest number of fragments encountered in this experiment.

currently much theoretical and experimental activity on this aspect of heavy-ion physics.[1-14]

In this experiment we examine the angular and momentum distributions of fragments emitted from relativistic central collisions between emulsion nuclei and heavy-ion projectiles ^{4}He and ^{16}O at 2.1 GeV/A and ^{40}Ar at 1.8 GeV/A (all beams have rigidity $pc/ze=5.7$ GV). The selection criterion we adopt to define a collision as "central" is that it exhibits an absence of projectile fragmentation, as we illustrate in Fig. 2. We have used Ilford G.5 emulsions for this study because they are sensitive to minimum-ionizing singly charged particles. We are able, therefore, to detect all fragmentation nuclei produced in heavy-ion collisions, irrespective of charge and velocity. By carrying out the experiment at $E\approx 2$ GeV/A we exploit the fact that the difference between the projectile and target rapidities (rapidity $y=\tanh^{-1}\beta_L$) is sufficiently large to effectively separate target from projectile fragmentation products. In order to exclude further from this experiment effects due to projectile fragmentation we have limited our measurements of angular distributions to ionizing tracks having restricted grain densities $g\geq 2g_{\min}$, corresponding to proton energies $E\leq 250$ MeV/A for $Z=1$ nuclei, and to track ranges $R\leq 4$ mm, corresponding to proton energies $E\leq 31$ MeV (244 MeV/c).

This study thus pertains to particle energies that are primarily associated with target fragmentation. Our ionization and range criteria are similar, but not identical, to those adopted by Jakobsson *et al.*[12,13] and Chernov *et al.*[14] in their emulsion studies of ^{16}O ($E=0.2$, 2.0 GeV/A) and ^{14}N($E=2.1$ GeV/A), respectively. Also, the limitations we have placed on track range and ionization, i.e., $E\leq 31$ and ≤ 250 MeV/A, closely match the sensitivity thresholds for ionizing tracks in AgCl crystals ($E_p\leq 28$ MeV and $E_{^4\mathrm{He}}\leq 200$ MeV/A) used by Schopper and colleagues in their measurements of the angular distributions of particles emitted from high-multiplicity reactions initiated by high-energy ^{4}He, ^{12}C, and ^{16}O nuclei.[9]

II. EXPERIMENTAL PROCEDURES

A. Detectors and scanning methods

Individual stacks of Ilford G.5 nuclear track emulsion were exposed to Bevatron-Bevalac beams of ^{4}He, ^{16}O, and ^{40}Ar at rigidity 5.7 GV, corresponding to $E=2.1$ GeV/A for the ^{4}He and ^{16}O beams, and 1.8 GeV/A for the ^{40}Ar beam. The emulsions were sensitive to singly charged relativistic particles which yielded ionization tracks with blob densities typically 20 blobs/100 μm at minimum ionization. Consequently, all fragmentation products, irrespective of charge and velocity, are detectable, a feature essential to this experiment since the recognition of projectile fragmentation is to be the basis for our selection criterion for central collisions. Both along-the-track and volume scanning techniques were used to locate events under 200× magnification. All track-coordinate measurements were made under oil immersion objectives, 1000× total magnification, using three-coordinate digitally encoded (1-μm readout) microscopes.

B. Criteria for central collisions

In the present experiment we define a central collision to be one that does not exhibit projectile fragmentation. To establish a criterion for the

selection of such collisions we refer to our previous investigation on the properties of projectile fragmentation. There, Heckman *et al.*[15] found that about 12% of the interactions of 2.1-GeV/A ^{12}C, ^{14}N, and ^{16}O beam nuclei in nuclear emulsion led to "pure" projectile fragmentation; interactions whose distinctive features are (i) all fragment nuclei are emitted in a narrow forward cone at near-beam velocities and (ii) no low-energy target-related particles are produced in the event (often termed an $n_h = 0$ type star, where n_h is the number of heavily ionizing tracks). Measurements of the angular distributions of $Z = 1$ and $Z = 2$ fragments of the projectile produced within the forward cone showed them to be compatible with a Gaussian distribution, with standard deviation widths $\theta_{SD} \approx 2.0°$ and 0.9°, respectively. These angular widths can be expressed in terms of $\sigma_{p_\perp}$, the standard deviation of the $p_\perp$ distributions of the emitted fragments:

$$\sin\theta_{SD} = \frac{\sigma_{p_\perp}}{p_B}\frac{A_B}{A_F}, \quad (1)$$

where p_B is the beam momentum, equal to $5.7Z_B$ GeV/c, and A_B and A_F are the mass numbers of the beam and fragment nuclei. The values of $\sigma_{p_\perp}$ evaluated from Eq. (1) for $Z = 1$ and $Z = 2$ fragments, taken to be, for simplicity, α particles and protons, produced by the fragmentation of $Z/A = \frac{1}{2}$ beam nuclei, are thus approximately 100 MeV/c and 190 MeV/c, respectively. The corresponding standard deviations in the longitudinal momentum distribution in the projectile frame, $\sigma_{p_\parallel} = 2^{-1/2}\,\sigma_{p_\perp}$ (assuming isotropy in this frame), are 71 and 130 MeV/c, in agreement with the measurements of $\sigma_{p_\parallel}$ by Greiner *et al.*,[16] who obtained $\sigma_{p_\parallel} = 69 \pm 4$ MeV/c for protons (distribution non-Gaussian, however) and $\sigma_{p_\parallel} = (130 \pm 1)$ MeV/c for ^{4}He.

The salience of the above discussion is that the topology of projectile fragments is well defined and conducive to efficient detection of projectile fragments in emulsion. Thus, the presence or absence of projectile fragmentation can be established on an event by event basis, which allows us to select interactions that are restricted to heavy emulsion nuclei Ag and Br, with impact parameters small enough to effectively occult the projectile nucleus. The events we designate as central collision events thus fulfill the following criteria:

(1) *For ^{4}He interactions*: No beam-velocity fragments are observed within 5° of the incident beam direction. This establishes an angular void of particles in the fragmentation cone approximately $2.5\theta_{SD}$ (protons).

(2) *For ^{16}O and ^{40}Ar interactions:* No beam-velocity fragments with $Z \geq 2$ are observed within 5° of the incident beam direction. This establishes an angular void approximately $5\theta_{SD}$ (^{4}He), and greater than this for higher fragment charges. One or two minimum-ionizing $Z = 1$ tracks are allowed in the 5° acceptance cone.

C. Measurements

For those heavy-ion interactions that satisfied the above criteria, the following procedures for the measurements of angle and track range were carried out for each interaction:

(1) The production angles were measured for all secondary fragments having a restricted grain density $g \geq 2g_{min}$, after correcting for the dip angle. A $Z = 1$ particle with $g \geq 2g_{min}$ has an energy $E \leq 250$ MeV/A. Angle measurements were carried out for a minimum of 6500 fragments for each beam.

(2) Both track ranges and angles were measured for a subset of at least 1200 fragments with ranges ≤ 4 mm. No minimum range cutoff was made, except that due to obscuration of short tracks (≈ 3 μm in length) at the point of interaction. A 4-mm range in emulsion corresponds to a proton (and ^{4}He) energy equal to 31 MeV/A.

(3) Each fragment measured under (1) was classified as to whether its potential range was less or greater than 4 mm. This visual estimate of potential range was made by the scanner-measurer by observing the grain density ($g \geq 10g_{min}$ for protons) and multiple scattering of the track in the pellicle containing the event. Fragments with estimated ranges less than 4 mm were classified as $E_p < 31$ MeV events, and were used to augment the statistics for the angular distribution of fragments with $R \leq 4$ mm, measured under (2).

III. ANALYTIC PROCEDURES

The fragment range and angular distributions presented in this paper are formed by summing over all of the events observed, rather than treating interactions individually. We make the practical assumption that the system we are considering, i.e., the ensemble formed by all the central collisions observed, is large enough to be considered statistically based on the hypothesis of equal *a priori* probabilities in phase space. This allows us to parametrize our distributions in the form of a modified Maxwell-Boltzmann distribution. This distribution, expressed in a covariant nonrelativistic form, in terms of the momentum P of the emitted fragments, with $c = 1$, is as follows:

$$d^2N/dPd\mu \propto P^2 \exp[-(P^2 - 2M\bar{\beta}_\parallel P\mu)/P_0^2], \quad (2)$$

where $\bar{\beta}_\parallel$ is normally considered to be the longitudinal velocity of the particle-emitting system $\mu = \cos\theta$, where θ is the laboratory angle between

the momentum of the fragment of mass M and the momentum of the initial projectile, and $P_0 = (2ME_0)^{1/2}$, where E_0 is the characteristic energy per particle in this hypothetical moving system.

Note that Eq. (2) does not contain an effective Coulomb barrier V_C. Support for this assumption comes from the work of Kullberg, Otterlund, and Resman,[17] who found that the spectrum of protons, $E < 10$ MeV produced in interactions, selected without bias, between cosmic-ray heavy ions and AgBr nuclei in emulsion was compatible only with low values of V_C, consistent with $V_C \approx 0$. Ciok *et al.*[18] also observed $V_C \approx 0$ was in good agreement for the range distribution of tracks $R \leq 4$ mm measured in proton-nucleus interactions at $E \geq 24$ GeV. The results of Sullivan *et al.*[19] also show the marked suppression of the effective Coulomb barrier to light fragment emission in 2.1 GeV/nucleon ^{16}O +Au collisions relative to that observed in 2.1 GeV p+Au collisions.

We now examine how Eq. (2) is modified when it is expressed in terms of range R and μ, the two quantities measured in this experiment. To good approximation, the R-β relation for Ilford emulsion is given by the power-law expression

$$\beta = k(Rz^2/A)^n, \tag{3}$$

where $k = 0.174$, $n = 0.29$, R is in mm, and z and A are the atomic and mass numbers of the fragment, respectively. In terms of β, Eq. (2) becomes

$$d^2N/d\beta d\mu \propto \beta^2 \exp[-(\beta^2 - 2\bar{\beta}_\parallel \beta\mu)/\bar{\beta}_0^2], \tag{4}$$

where $\bar{\beta}_0 = (2E_0/M)^{1/2}$. If we transform this distribution to a distribution of track ranges R, the distribution in R-μ space becomes

$$d^2N/dRd\mu \propto (z^2/A)^{3n} R^{3n-1} \times \exp[-(k^2R^{2n} - 2\beta_\parallel kR^n\mu)/\beta_0^2], \tag{5}$$

where

$$\beta_\parallel = \bar{\beta}_\parallel (A/z^2)^n \quad \text{and} \quad \beta_0 = \bar{\beta}_0 (A/z^2)^n. \tag{6}$$

It follows that the parameter we shall denote as

$$\chi_0 = \beta_\parallel/\beta_0 = \bar{\beta}_\parallel/\bar{\beta}_0, \tag{7}$$

which is the ratio of the longitudinal velocity of the center of mass $\beta_\parallel$ to the characteristic spectral velocity β_0 of the fragmenting system, is common to both the velocity and range spectra, and is independent of (A, z).

Thus the longitudinal velocity $\beta_\parallel$ and spectral velocity β_0 that characterize the *range* spectrum of unidentified fragments [Eq. (5)] are related to the corresponding quantities for the *velocity* spectrum [Eq. (4)] for any fragment (A, z) by the factor $(A/z^2)^n$, where n is the range-velocity index. Therefore the parameters β_0 and $\beta_\parallel$, the only quantities we may deduce from our range and angle data, can be evaluated from the velocity distribution [Eq. (4)] for any value of A/z^2 through Eq. (6). In our analysis, β_0 and $\beta_\parallel$ were actually evaluated using the velocity distribution [Eq. (4)] assuming $A/z^2 = 1$, for which $\bar{\beta}_0 \equiv \beta_0$ and $\bar{\beta}_\parallel \equiv \beta_\parallel$. The key point here is that the two range-distribution parameters $\beta_\parallel$ and β_0 can only be identified as fragment velocities $\bar{\beta}_\parallel$ and $\bar{\beta}_0(E_0)$ when the isotopic distribution of stopped fragments is known. By fitting the measured range and angle data to evaluate $\beta_\parallel$ and β_0 we are effectively testing how well such data can be described given the following assumptions:

(i) The observed range and angle distributions are interpretable in terms of a single Maxwellian-range (velocity) distribution.

(ii) The isotopic distribution of fragments is dominated by one species, i.e., protons, thereby minimizing any significant difficulties in defining β_0 in the Maxwell distribution [Eq. (4)].

(iii) To the extent that (ii) is satisfied, the $\beta_\parallel$ and β_0 parameters that characterize the range and angular distributions are the same as those that describe the velocity distribution for protons.

(iv) The effective Coulomb barrier V_C for proton emission is vanishingly small for the central high-energy-deposition collisions selected in this experiment.

Physical interpretations of the parameters β_0 and $\beta_\parallel$ (we shall omit the bar notation henceforth) can be clarified if we introduce $\beta^2 = \beta_L^2 + \beta_T^2$, where β_L and β_T are the longitudinal and transverse components of $\vec{\beta} = \vec{P}/M$, to Eq. (4), which then becomes factorable:

$$d^2N/\beta_T d\beta_T d\beta_L \propto \exp(-\beta_T^2/\beta_0^2)\exp[-(\beta_L - \beta_\parallel)^2/\beta_0^2]. \tag{8}$$

Thus, we note that the marginal probability distribution for β_L ($\approx$ rapidity y) is Gaussian, with

$$\langle \beta_L \rangle = \beta_\parallel \quad (\text{1st moment of the } \beta_L \text{ distribution}) \tag{9a}$$

and

$$\sigma^2(\beta_L) = \beta_0^2/2 = E_0/M \quad (\text{variance of the } \beta_L \text{ distribution}). \tag{9b}$$

This variance can also be expressed in the form $\sigma^2(\tau) = \tau/M_n$, where the equivalent "temperature" of the system is τ (MeV/A) and M_n is the nucleon mass.

The observed distributions of velocity β and angle $\mu = \cos\theta$, for fragments produced by each of the incident projectiles were binned in a β-μ matrix, normally 20×10 in size, and fitted to Eq. (4) (with $A/z^2 = 1$) by use of the minimizing rou-

tine MINUIT,[20] assuming statistical errors $\sim N^{-1/2}$, to determine $\beta_{\parallel}$ and β_0. The errors quoted for these parameters correspond to a change of 1.0 in the value of χ^2 for the fit. The integration of Eq. (4) over the variables β and $\mu = \cos\theta$ leads to the following expression for N_{ij}, the expected number of fragments bounded by the ith interval of β, $\beta_i \leq \beta \leq \beta_{i+1}$ and the jth interval of μ, $\mu_j \leq \mu \leq \mu_{j+1}$:

$$N_{ij} \propto F(\mu_{j+1}) - F(\mu_j) + G(\mu_{j+1}) - G(\mu_j), \tag{10}$$

where

$$F(\mu) = [\exp(\chi_0^2 \mu^2)]\{\exp[-\chi_0^2(\beta_i/\beta_{\parallel} - \mu)^2] - \exp[-\chi_0^2(\beta_{i+1}/\beta_{\parallel} - \mu)^2]\},$$

$$G(\mu) = \sqrt{\pi}\chi_0\mu[\exp(\chi_0^2\mu^2)]\{\mathrm{erf}[\chi_0(\beta_{i+1}/\beta_{\parallel} - \mu)] - \mathrm{erf}[\chi_0(\beta_i/\beta_{\parallel} - \mu)]\},$$

and

$$\chi_0 = \beta_{\parallel}/\beta_0.$$

The angular distribution derived from Eq. (4) for fragments in the ith interval $\beta_i \leq \beta \leq \beta_{i+1}$ is

$$\frac{dN}{d\mu} \propto [\exp(\chi_0^2\mu^2)] \times \{h(\beta_i) - h(\beta_{i+1}) - 2^{-1}\sqrt{\pi}(1 + 2\chi_0^2\mu^2) \times [g(\beta_i) - g(\beta_{i+1})]\}, \tag{11}$$

where

$$h(\beta) = \chi_0(\beta/\beta_{\parallel} + \mu)\exp[-\chi_0^2(\beta/\beta_{\parallel} - \mu)^2]$$

and

$$g(\beta) = \mathrm{erf}[\chi_0(\beta/\beta_{\parallel} - \mu)].$$

Note that when the angular distribution is measured without regard to fragment velocity, $dN/d\mu$ becomes a function of the single fitting parameter $\chi_0 = \beta_{\parallel}/\beta_0$ only. In this case, the ratio of the number of fragments in forward to backward hemispheres, F/B is given by

$$F/B = \frac{1 + \mathrm{erf}\chi_0}{1 - \mathrm{erf}\chi_0}. \tag{12}$$

To first order in χ_0, $dN/d\mu$ and F/B can be expressed as

$$dN/d\mu \approx \exp\left[\frac{4}{\sqrt{\pi}}\chi_0\mu\right], \tag{13a}$$

$$F/B \approx \exp\left[\frac{4}{\sqrt{\pi}}\chi_0\right]. \tag{13b}$$

Hence,

$$dN/d\mu \approx (F/B)^{\mu}, \tag{13c}$$

$$dN/d\theta \approx \sin\theta(F/B)^{\cos\theta}. \tag{13d}$$

For the values of F/B we shall obtain in this experiment ($F/B \lesssim 2.5$), Eq. (13c) is a good approximation of the exact expression $dN/d\mu$ [Eq. (11)].

These analytical procedures are similar to those embodied in the two-step vector model that is widely used to interpret the production of the residual target by recoil techniques.[21] In this model it is assumed that the velocity of a product nucleus is given by $\vec{V}_{\mathrm{lab}} = \vec{v} + \vec{V}$, where $\vec{v}$ is the velocity of the excited system produced on impact of the projectile and target and $\vec{V}$ is the velocity imparted to the product nucleus in the deexcitation stage. For the case where $\vec{V}$ has a Maxwell-Boltzmann distribution, the commonly used quantity $\eta_{\parallel} = \langle v_{\parallel}/V \rangle$ and $\chi_0 = \beta_{\parallel}/\beta_0$ used here are related by the expression $\eta_{\parallel} = 2\pi^{-1/2}\chi_0$.

IV. EXPERIMENTAL RESULTS

A. Prong-number distribution

Figure 3 presents the distributions of prong number per event N_p for the interactions of each heavy-ion beam selected under the criteria stated in Sec. II B. The distributions thus pertain to charged prongs having restricted grain densities $g \geq 2g_{\min}$, i.e., equivalent to proton energies ≤ 250 MeV, emitted

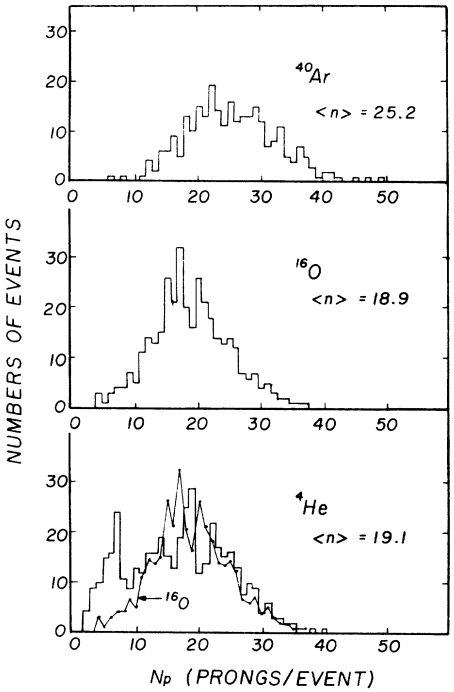

FIG. 3. Distribution of number of prongs (fragments) per event emitted from central collisions with restricted grain densities $g > 2g_{\min}$, corresponding to proton energies $E_p < 250$ MeV. Beam energies are 2.1 GeV/A for ^{4}He and ^{16}O, and 1.8 GeV/A for ^{40}Ar. The mean number of prongs/event $\langle n \rangle$ are indicated. The CNO peak ($N_p \sim 6$–8) is not included in the value of $\langle n \rangle$ for ^{4}He.

from events selected only when the projectile was fully occulted by the target nucleus. If we first consider the multiplicity distributions of prongs arising from ^{40}Ar and ^{16}O collisions, we note that each distribution shows a single maximum and is approximately symmetric about its mean prong number. In contrast, the N_p distribution for ^{4}He projectiles shows two maxima, one in the region of $N_p = 6$ to 8, and the other at $N_p \approx 19$. We attribute the low-prong-number peak to collisions between the ^{4}He projectile and CNO (light) nuclei, and the high-number peak to collisions with AgBr (heavy) nuclei because He can be occulted in CNO as well as in AgBr collisions. The absence of this CNO peak in the ^{16}O and ^{40}Ar prong distributions indicates that nonoccultation of the projectile by the target nucleus occurring in collisions between these projectile nuclei and light CNO targets invariably shows evidence for projectile fragmentation.

We argue, therefore, that the prong distributions observed for ^{40}Ar and ^{16}O projectiles are due to interactions with heavy emulsion nuclei only, principally Ag and Br. Similarly, the ^{4}He events having $N_p > 9$ are also attributable to interactions with Ag and Br. We superimposed the ^{16}O prong distribution, normalized for $N_p > 9$, upon the ^{4}He prong distribution to illustrate the similarity between these distributions. The mean values of these distributions $\langle n \rangle$ are statistically equal, i.e., 19.1 for ^{4}He (after eliminating the CNO peak) and 18.9 for ^{16}O, and they have comparable widths, σ, equal to 6.6 and 6.2, respectively. The prong distribution of ^{40}Ar has a greater mean prong number and dispersion, 25.2 ± 7.2, than is observed for the ^{4}He and ^{16}O distributions, indicative of increased excitation energies in the ^{40}Ar collisions.

Thus, by eliminating prong numbers $N_p \leq 9$ from the ^{4}He data, we have limited the interactions of relativistic ^{4}He, ^{16}O, and ^{40}Ar nuclei in nuclear emulsions in the present study to near-central collisions with Ag and Br having little, if any, remaining contribution to the data from collisions with lighter emulsion nuclei.

B. Salient features of the angular distribution of prongs (fragments)

In Table I we summarize the angular distribution data for fragments produced by each beam nucleus. The data are catalogued according to the energy (or range) window of the fragments, i.e., $E_p < 31$ MeV, $E_p < 250$ MeV, and $R < 4$ mm. (The notation "$E_p <$" will be used to signify that the given energy limit is estimated by inspection of the grain density and multiple scattering of the fragment. Data identified by $R \leq 4$ mm, for which $\epsilon = E/A = 31$ MeV/A for protons and ^{4}He, will signify that the data are based on range measurements.) Included in the tabulations are the number of prongs that comprise the data base, and their division into forward and backward hemispheres. The data given in Table I(a) show a significant decrease in the amplitude of the low-energy component, $E_p < 31$ MeV, as the mass of the incident ion increases. For a ^{4}He projectile, 67% of the fragments produced in central collisions are < 31 MeV, whereas this fraction is reduced by about a factor of 2, to $\approx 30\%$, for ^{40}Ar projectiles. Although the absolute number in the forward and backward hemisphere varies, the forward-backward ratios for the $E_p < 31$ MeV data (Table I) and the $R \leq 4$ mm subset of this data, are virtually independent of the mass of the projectile. The F/B ratio tends, however, to become smaller as A_{beam} increases. For the higher-energy window, $E_p < 250$ MeV, this slight trend of F/B is reversed, and this ratio for ^{40}Ar increases dramatically, relative to the (approximately equal to one another) F/B ratios for ^{4}He and ^{16}O. Note, however, that for the projectiles used for these data, the number of back-hemisphere prongs per event, $N_p(\theta > 90°)/N_{\text{int}}$, is nearly constant, being 6.8, 6.7, and 7.1

TABLE I. Summary of the measurements on the angle and range distributions. N_{int} is the number of interactions and N_p denotes the number of prongs (fragments) observed. F/B is the forward/backward ratio.

Beam	N_{int}	N_p(total)	$N_p(\theta < 90°)$	$N_p(\theta < 90°)$	F/B
(a) Angular distributions only, $E < 31$ MeV ($E < 250$ MeV)					
^{4}He	335	4462(6666)	2649(4397)	1813(2269)	$1.46 \pm 0.04(1.94 \pm 0.05)$
^{16}O	352	3491(6644)	2015(4291)	1476(2353)	$1.37 \pm 0.05(1.82 \pm 0.06)$
^{40}Ar	270	2045(6832)	1170(4902)	875(1930)	$1.34 \pm 0.06(2.54 \pm 0.07)$
(b) Range and angular distributions, $R \leq 4$ mm					
^{4}He	123	1396	811	581	1.40 ± 0.08
^{16}O	308	2471	1408	1063	1.32 ± 0.05
^{40}Ar	240	1459	817	642	1.27 ± 0.07

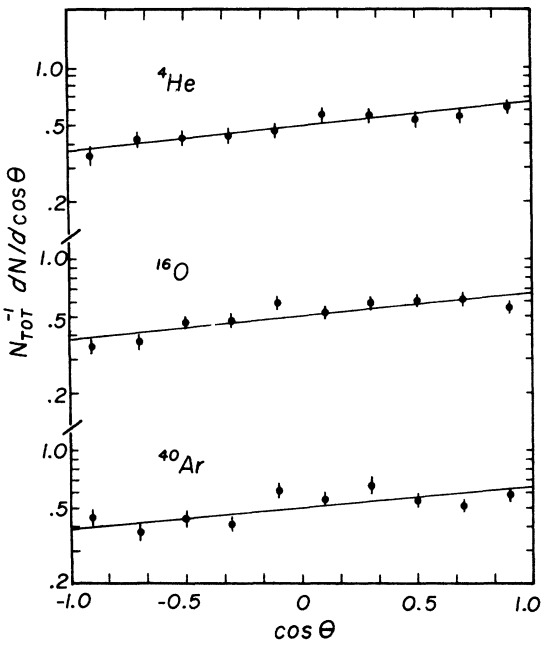

FIG. 4. Angular distributions of fragments with ranges $R \leq 4$ mm emitted from central collisions between AgBr target nuclei and ^{4}He, ^{16}O, and ^{40}Ar projectiles. The beam rigidity (pc/ez) is 5.7 GV for all ions. The curves drawn through the data are least-squares fits to Eq. (10). The parameters $\beta_{\parallel}$ and β_0 are given in Table II.

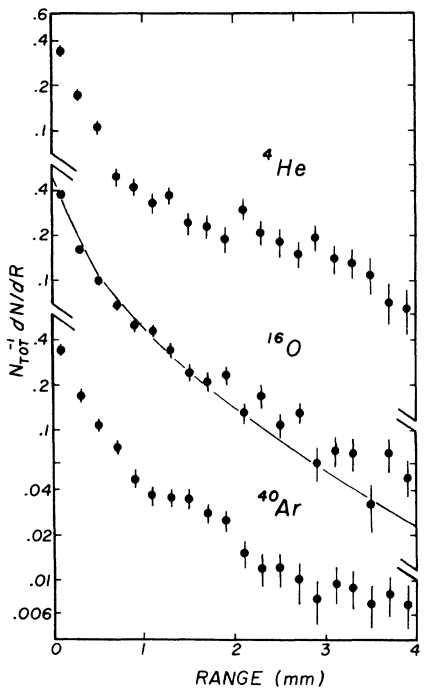

FIG. 5. Range distributions for fragments for ranges $R \leq 4$ mm emitted from central collisions in emulsion. Projectiles are ^{4}He, ^{16}O, and ^{40}Ar with rigidity 5.7 GV. The fitted range distribution, Eq. (10), is illustrated for the ^{16}O data. The parameters $\beta_{\parallel}$ and β_0 are given in Table II.

for ^{4}He, ^{16}O, and ^{40}Ar, respectively. The changes in the F/B ratios are thus primarily attributable to changes in the fragment-production cross sections in the forward hemisphere.

C. Range and angular distributions, $R \leq 4$ mm

Figures 4 and 5 present the angular and range distributions observed for fragments with ranges $R \leq 4$ mm emitted from the previously described central collisions produced by the ^{4}He, ^{16}O, and ^{40}Ar projectiles. Tabulated in Table II are the range-velocity parameters $\beta_{\parallel}$ and β_0, and the quantity χ_0 evaluated therefrom, obtained by least-squares fits of the data to Eq. (10). The two-parameter fitted curves are superimposed on the angular distribution data (Fig. 4) and on the range spectrum of fragments observed in ^{16}O collisions (Fig. 5). The principal feature of these data is the near independence of the normalized

TABLE II. Range-velocity parameters $\beta_{\parallel}$, β_0, and $\chi_0 = \beta_{\parallel}/\beta_0$ versus range interval for $R \leq 4$ mm. ϵ is the proton energy corresponding to range R.

Range (mm)	ϵ (MeV)		^{4}He	^{16}O	^{40}Ar
0–4	0–31	$\beta_{\parallel}$	0.016 ± 0.004	0.015 ± 0.002	0.012 ± 0.002
		β_0	0.117 ± 0.002	0.115 ± 0.002	0.117 ± 0.002
		χ_0	0.14 ± 0.04	0.13 ± 0.02	0.10 ± 0.02
0–1	0–14	$\beta_{\parallel}$	0.010 ± 0.002	0.012 ± 0.002	0.014 ± 0.004
		β_0	0.105 ± 0.003	0.104 ± 0.003	0.110 ± 0.003
		χ_0	0.10 ± 0.02	0.11 ± 0.02	0.13 ± 0.04
1–4	14–32	$\beta_{\parallel}$	0.030 ± 0.011	0.016 ± 0.005	0.016 ± 0.003
		β_0	0.169 ± 0.015	0.122 ± 0.004	0.143 ± 0.012
		χ_0	0.18 ± 0.07	0.13 ± 0.04	0.11 ± 0.02

range and angular distributions on the mass of the projectile, as indicated by the statistical constancy of the parameters $\beta_{\parallel}$ and β_0 (Table II).

Important differences between the data and the two-parameter Maxwell-Boltzmann distribution [Eq. (4)] are evident, however. We first refer to Fig. 4, which shows the angular distribution of fragments having $R \leq 4$ mm, plotted as a function of incident ion. A close inspection of $dN/d\cos\theta$ for $\cos\theta > 0$ shows that its slope is nearly zero, compatible with isotropy in the laboratory, corresponding to $\beta_{\parallel} \approx 0$. The angular distributions systematically tend to be nearly more isotropic in the forward hemisphere (in the laboratory) relative to the backward hemisphere. We shall elaborate on this point later. Second, as illustrated by the ^{16}O data (Fig. 5), the computed range distributions are systematically lower than the data for ranges $R > 2$ mm. Such differences are consistent with the well-documented experimentally observed excess of energetic fragments, relative to that expected from particle-evaporation models.[22] The differences between the data and fitted curves therefore indicate that unique values of $\beta_{\parallel}$ and β_0 cannot account for the shape of the range spectra. To examine how $\beta_{\parallel}$ and β_0 depend on range, we also performed fits to the range-angle data for the range intervals $0 \leq R \leq 1$ mm, equivalent to proton energies $\epsilon \leq 14$ MeV/A, and $1 \leq R \leq 4$ mm, equivalent to $14 \leq \epsilon \leq 31$ MeV/A. The results are included in Table II. They show that as the range, hence, energy, of the fragment increases, both $\beta_{\parallel}$ and β_0 increase. The ratios χ_0, however, appear to remain constant, all values being compatible with a mean value $\langle \chi_0 \rangle = 0.11 \pm 0.01$. The longitudinal velocities of the particle-emitting system $\beta_{\parallel}$ are small and, within the accuracy of the measurements, independent of projectile. As we shall discuss later, the values of $\beta_{\parallel}$ observed here are equal to those measured for low-energy fragment-emitting systems produced in proton-nucleus collisions over a broad range of energies. We also point out that the temperatures τ implied by the velocities $\beta_0 = (2\tau/M_n)^{1/2}$ are typically 6–7 MeV/A, characteristic of the binding energies of nuclei and also compatible with the temperatures associated with projectile fragmentation.[16,23]

Figure 6 presents the range-angle data in the rapidity variable $y \approx \beta_L$, where β_L is the longitudinal component of the quantity $\vec{\beta}$, obtained from Eq. (3), assuming $z^2/A = 1$. By equating each fragment range to an equivalent proton (or ^4He) velocity, we obtain a rapidity distribution that is reproduced well by the two-parameter Maxwell-Boltzmann distribution [Eq. (8)]. The mean value $\langle y \rangle \approx \beta_{\parallel}$ is indicated for each distribution, as is the standard deviation $\sigma_y = \beta_0/\sqrt{2} = (\tau/M_n)^{1/2}$. The cut-

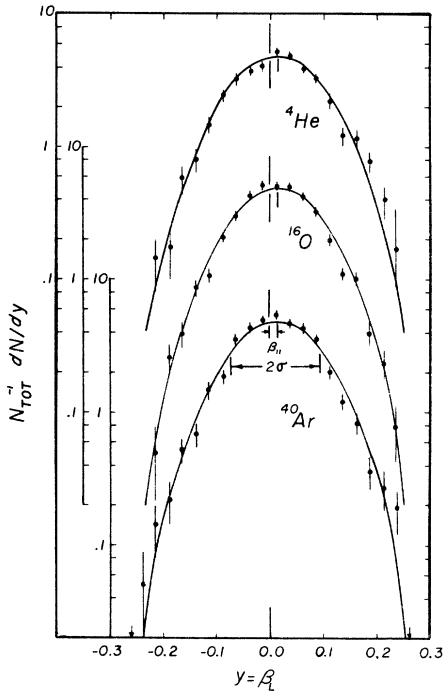

FIG. 6. Rapidity distributions $y = \beta_L$ of fragments with ranges $R \leq 4$ mm, assuming $A/z^2 = 1$. Cutoff values of $\beta_L = 0.260$ are indicated by the arrows on the abscissa. Values of $\beta_{\parallel}$ and $\beta_0 = \sqrt{2}\sigma$ are given in Table II. The energies of the projectiles indicated are 2.1 GeV/A (^4He and ^{16}O) and 1.8 GeV/A (^{40}Ar).

off values of y at $R = 4$ mm are ± 0.260, which are indicated by the arrows in the figure. The average standard deviation of the three rapidity distributions is $\langle \sigma_y \rangle = 0.082 \pm 0.001$, corresponding to a longitudinal momentum $P_L = 77$ MeV/c per nucleon.

D. Angular distributions $E_p < 31$ MeV

As described in Sec. II C, the scanner-measurer made, by visual inspection only, an estimate of the potential range of all fragments based on the grain density and multiple scattering of the track, and tagged those events with potential range ≤ 4 mm. Under this criterion, protons and ^4He nuclei with $E_p \leq 31$ MeV/A were identified. When a sample of the tagged fragments was followed to the end of their ranges, or to a maximum of 4 mm, we found that approximately 85% of the tracks came to rest within a 4-mm range. The angular distribution for tagged events was also observed to differ little from that for fragments whose ranges were actually measured to be ≤ 4 mm.

The angular distributions observed for fragments with energies $E_p < 31$ MeV, based on estimated range, produced by each of the incident projectiles, are shown in Fig. 7. The distributions are pre-

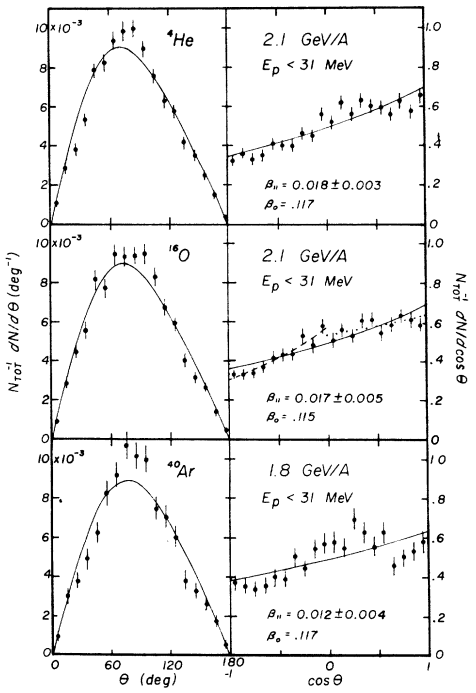

FIG. 7. Angular distributions for fragments $E_p < 31$ MeV emitted from central collisions observed in nuclear emulsion. Solid curves are fits of the data to Eq. (10), $-1 \leq \mu \leq 1$, using the parameters indicated. The dashed and dotted curves are fits to the data, for the backward and forward hemispheres, respectively.

sented as functions of both θ and $\cos\theta$. Drawn through the data are curves derived from the fitted Maxwell-Boltzmann distributions. Because these angular distributions were taken without knowledge of particle ranges subject only to the condition that $E_p < 31$ MeV, we found that the minimum χ^2 fits did not yield unique values for $\beta_\parallel$ and β_0, but rather gave values of $\beta_\parallel$ and β_0 that were linearly coupled. Thus, we chose to fix β_0 at the value determined previously from the range-angle data and evaluate $\beta_\parallel$. The values of $\beta_\parallel$ thus obtained are indicated in Fig. 7, along with the appropriate β_0's taken from Table II. The longitudinal velocities $\beta_\parallel$ derived from the angular distributions shown in Fig. 7 are in statistical agreement with the $\beta_\parallel$ parameter obtained from the range-angle data, although a small systematic increase in $\beta_\parallel$ is indicated. This increase is consistent with the inclusion of misidentified fragments in the sample of events having ranges > 4 mm that were excluded from the previously described data where the ranges were accurately measured.

As do the angular distributions for fragments with $R \leq 4$ mm (Fig. 6), the distributions of $dN/d\cos\theta$ consistently show greater isotropy in the forward, relative to backward, hemisphere. In the case of the ^{16}O data, the fits to the data in the backward and forward hemispheres are indicated, which illustrates the marked difference between the angular distributions for $\cos\theta < 0$ and $\cos\theta > 0$. In Table III the fitted parameters $\chi_0 = \beta_\parallel/\beta_0$ that characterize the angular distributions in the backward, forward, and combined hemispheres for the $E_p < 31$ MeV data are listed. The angular spectra of the low-energy fragments, when examined in either hemisphere, continue to exhibit projectile independence. Qualitatively, the spectrum for each projectile shows that $\chi_0(-1 < \mu < 0)$ is about 0.3, whereas $\chi_0(0 < \mu < 1)$ is consistent with zero. Thus, the diminution of the ratio $\chi_0 = \beta_\parallel/\beta_0$ as one proceeds from the backward to forward hemispheres indicates, we believe, marked differences in the physical processes that contribute to low-energy fragment emission in the two hemispheres at projectile energies ≈ 2 GeV/A.

If we now refer to the angular distributions plotted as $dN/d\theta$ versus θ, the "break" in the $dN/d\cos\theta$ distribution near $\cos\theta = 0$ leads to a general excess of particles near 90° when compared with the Maxwell-Boltzmann fit based on fits over the

TABLE III. Angular distribution parameter $\chi_0 = \beta_\parallel/\beta_0$ for the backward, forward, and combined hemispheres as a function of energy window E_p and projectile. Values of χ_0 given by Eq. (13b), applicable to the interval $-1 < \mu < 1$, are also tabulated.

E_p (MeV)	$\mu = \cos\theta$	^{4}He	^{16}O	^{40}Ar
0–31	$-1 < \mu < 0$	0.25 ± 0.07	0.31 ± 0.10	0.28 ± 0.11
	$0 < \mu < 1$	0.05 ± 0.05	0.07 ± 0.07	−0.07 ± 0.10
	$-1 < \mu < 1$	0.16 ± 0.02	0.15 ± 0.04	0.11 ± 0.03
	$\chi_0(F/B)$	0.168	0.139	0.130
0–250	$-1 < \mu < 0$	0.31 ± 0.08	0.37 ± 0.09	0.52 ± 0.06
	$0 < \mu < 1$	0.24 ± 0.04	0.18 ± 0.03	0.39 ± 0.06
	$-1 < \mu < 1$	0.28 ± 0.03	0.26 ± 0.02	0.41 ± 0.02
	$\chi_0(F/B)$	0.294	0.265	0.413

interval $-1 < \mu < 1$. The measured distributions $dN/d\theta$, however, are smoothly varying, with maxima at 70–75°, and do not display statistically significant fine structure indicative of well-defined collective phenomena.

E. Angular distributions $E_p < 250$ MeV

The angular distributions $dN/d\theta$ and $dN/d\cos\theta$ for all fragments with $g \geq 2g_{\min}$ are given in Fig. 8. The experimental data were fitted to the angular distribution given by Eq. (11) to obtain the parameter χ_0. The values of χ_0 for the $E_p < 250$ MeV data are given in Table III for backward, forward, and combined hemispheres, the latter fit superimposed on the data shown in Fig. 8. By extending the energy window from $E_p < 31$ to $E_p < 250$ MeV, the sharp break between the angular distributions has been noticeably reduced. However, the effect persists, largely owing to the low-energy component, as indicated by the systematically higher values of χ_0 $(-1 < \mu < 0)$ relative to χ_0 $(0 < \mu < 1)$. The fits to the angular distributions in the forward and backward hemispheres are indicated for fragments produced by ^{16}O projectiles.

In contrast to the angular spectra for the low-energy fragments, the angular distribution for fragments with $E_p < 250$ MeV do exhibit a dependence on projectile mass. Whereas the spectral shapes for the ^{4}He and ^{16}O data are indistinguishable, i.e., the χ_0's are equal within their errors, the angular distribution of fragments from ^{40}Ar interactions clearly shows the effects of increased mass number of the projectile. This difference is attributable to a large increase in the number of fragments produced by ^{40}Ar projectiles between $E_p = 31$ and 250 MeV, which leads to an approximate doubling of the F/B ratio for this projectile as E_p increases from 31 to 250 MeV (Table I). With an increase in the energy window of the fragments, we note that the maxima in the $dN/d\theta$ distributions are at smaller angles, the maxima having decreased from 70–75°, when $E_p < 31$ MeV, to 55–60° when $E_p < 250$ MeV.

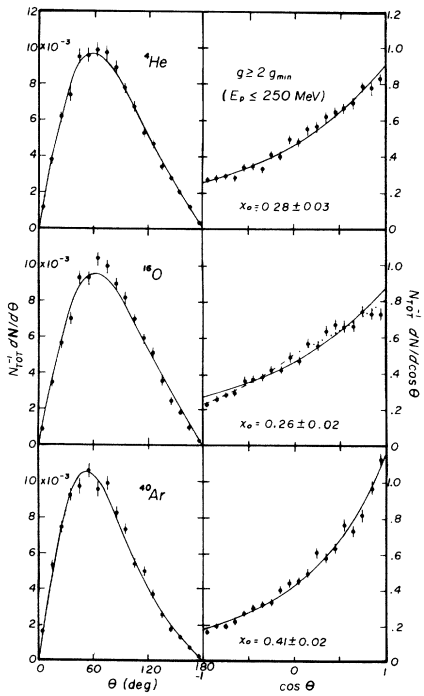

FIG. 8. Angular distributions for fragments with $g \leq 2\,g_{\min}$, $E_p < 250$ MeV, emitted from central collisions observed in nuclear emulsion. See caption for Fig. 7 for identification of the plotted curves.

The one-parameter Maxwellian fits to the data shown in Fig. 8 give χ^2 values typically 1–2/data point, hence, are satisfactory representations of the observations. Included in Table III are the values of χ_0 evaluated from the approximate expression for this quantity in terms of the F/B ratio [Eq. (13b)]. The agreement between χ_0 (F/B) and the value of χ_0 deduced by least-squares fitting is excellent. The expressions for $dN/d\mu$ and $dN/d\theta$ [Eqs. 13(c) and 13(d)] also approximate well a Maxwell-Boltzmann distribution that is characterized by the parameters $\beta_\parallel$ and $\beta_0 = (2\tau/M_n)^{1/2}$, for which the observed F/B ratios in the laboratory frame are simply related to $\beta_\parallel$ and β_0 by the Eqs. (12) or (13b).

V. DISCUSSION

One of the principal objectives of this experiment was to discover whether or not the interactions between nuclei at relativistic energies, selected on the basis that the collisions were near central, show phenomena significantly different from that observed in previous experiments involving either heavy-ion or proton projectiles. Existing data with which we can best compare our observations are for the low-energy fragments $E \lesssim 30$ MeV/A. We recall that the low-energy spectra produced by ^{4}He, ^{16}O, and ^{40}Ar beam nuclei observed in this experiment are distinguished by the following characteristics:

(i) The angular and range distributions are, within the experimental errors, independent of the mass of the projectile.

(ii) The longitudinal velocities $\beta_\parallel$ of the particle-emitting systems are low, typically 0.014 ± 0.002, with little dependence on the mass of the projectile.

(iii) The ratio $\chi_0 \equiv \beta_\parallel/\beta_0$ appears to be constant, independent of projectile mass and energy (range) of the fragments.

In Table IV we have tabulated a representative sample of published data on the forward-backward ratios F/B and longitudinal velocities $\beta_{\parallel}$. These parameters describe the qualitative features of the spectra of low-energy fragments emitted from both selected and unselected interactions between heavy-ion and proton projectiles, and targets of Ag and heavy emulsion nuclei [Ag(Br) can be identified by selecting interactions with $n_h \gtrsim 10$]. Because $\beta_{\parallel}$ is a model-dependent parameter, we shall concentrate on the measured F/B ratios in our comparison. We note, nonetheless, that the longitudinal velocities $\beta_{\parallel}$ are all low, typically $0.01 < \beta_{\parallel} < 0.02$, irrespective of projectile, energy, and (possibly) fragment. If we compare the results of the emulsion experiments in which the fragments were identified by range only (the range intervals for this experiment and Refs. 14, 24, and 26 are comparable), we find the mean of the F/B ratios observed in nucleus-nucleus collisions is 1.41 ± 0.03, whereas it is equal to 1.32 ± 0.05 in proton-nucleus collisions. A tentative conclusion would be that a slight increase in the F/B ratios of the low-energy fragments is indicated as one proceeds from light to heavy projectiles, but this reasoning is obscured by the observation that the F/B ratios for ^{40}Ar and proton projectiles are in close agreement, and that our data show, in fact, an opposite trend in the F/B ratios with projectile mass. The agreement between this experiment and the results of Chernov *et al.*,[14] who observe $F/B = 1.40 \pm 0.06$ for ^{14}N ions at 2.1 Gev/A, is of particular interest in that their data were obtained from an unselected sample of interactions. Based on our data, only about one-third of their ^{14}N interactions would be central collisions of the type selected for our experiment. Thus, we find no evidence for a dependence of the forward/backward asymmetry in the low-energy fragment distributions on the presence or absence of projectile fragmentation in the interaction. We may infer, therefore, that the velocity of the particle-emitting system does not depend sensitively on the impact parameter of the collision.

The F/B ratios measured for He fragments $E_{\mathrm{He}} \leq 50$ MeV[27] and ≤ 80 MeV,[22] produced by protons at $E = 2$, 3, and 5.5 GeV, as a group, are relatively low in comparison to the average of the F/B ratios tabulated. Hyde, Butler, and Poskanzer[22] noted the low average velocity of the emitting sys-

TABLE IV. Comparison of the results of this experiment and representative literature values of the F/B ratio and $\beta_{\parallel}$ for fragment spectra $E \leq 31$ MeV/A produced in nucleus-nucleus and proton-nucleus collisions. Targets denoted as AgBr refer to emulsion experiments where target identification was made by the criterion $n_h \gtrsim 7$, those denoted as CR refer to cosmic rays.

Beam	E_{beam} (GeV/A)	Target	Fragment	F/B	$\beta_{\parallel}$	Ref.
			Nucleus-nucleus			
^{4}He	2.1	AgBr	$R \leq 4$ mm	1.46 ± 0.04	0.016 ± 0.004	This exp.
^{16}O	2.1	AgBr	$R \leq 4$ mm	1.37 ± 0.05	0.015 ± 0.002	This exp.
^{40}Ar	1.8	AgBr	$R \leq 4$ mm	1.34 ± 0.06	0.012 ± 0.002	This exp.
^{14}N	2.1	Emul.	$R \leq 3$ mm	1.40 ± 0.06		14
^{16}O	2.1	AgBr	$E_p^{\mathrm{c.m.}} \leq 25$ MeV		0.022 ± 0.001	13
^{16}O	2.1	AgBr	$E \leq 11$ MeV/A	1.12 ± 0.08		12
CR	$2 < E < 15$	Emul.	$R \leq 3.5$ mm	1.48 ± 0.09	0.026[a]	24
CR	$E > 1.5$	AgBr	$g \geq 6g_{\mathrm{min}}$		0.029[a]	25
			p-nucleus			
p	2.2	Emul.	$R \leq 3.5$ mm	1.32 ± 0.05		26
p	2	Emul.	$E_{\mathrm{He}} \leq 50$ MeV	1.15 ± 0.09	0.015	27
p	3	Emul.	$E_{\mathrm{He}} \leq 50$ MeV	1.09 ± 0.11	0.020	27
p	5.5	Ag	$E_{\mathrm{He}} \leq 80$ MeV	1.17	0.003	22
p	24	Emul.	$10 < R < 2745$ μm	1.16 ± 0.07		28
CR	10^1–10^5	Emul.	$10 < R < 2745$ μm	1.28 ± 0.09		18
CR		Emul.	^{8}Li	1.5	0.016	29
p	5.5	Ag	$^{6\text{-}8}$Li	1.36	0.008 ± 0.002	22
p	9	Emul.	^{8}Li	1.44 ± 0.20	0.013 ± 0.003	30
p	9	Emul.	^{8}Li	1.7	0.015	31
p	19	Emul.	^{8}Li	1.65	0.015	32
p	24	Emul.	^{8}Li	1.54 ± 0.22	0.015 ± 0.003	30
p	25	Emul.	^{8}Li	1.20 ± 0.05	0.008	33

[a] Evaluated from $\beta = \beta_0 \cos\theta_{1/2}$, where $\theta_{1/2}$ is median angle of fragments in laboratory system, and β_0 is assumed to be ≈ 0.16.

tem $\beta_{\parallel}$ and the suppressed F/B ratio for the He fragments, and suggested these effects were in keeping with the ease of emission of the fragments from nuclei at all levels of excitation. Pertinent to this observation, Jakobsson *et al.*[12] also commented on the high degree of isotropy of He nuclei with $7.5 \leq E \leq 65$ MeV/A emitted from interactions between AgBr and 2.0 GeV/A projectiles—a degree of isotropy comparable to the evaporation like spectra observed for low-energy hydrogen, $E \leq 11$ MeV/A and He, $E \leq 7.5$ MeV/A. The emission of ^{8}Li (which are uniquely identified in emulsion by the $^{8}\mathrm{Li} \rightarrow {}^{8}\mathrm{Be} \rightarrow 2\alpha$ decay chain) in proton-nucleus collisions does not show the anomalous effects suggested by the He data.[29] These augmented by a number of similar experiments over a broad range of proton energies, are in remarkably good agreement with the F/B and $\beta_{\parallel}$ parameters observed in the present experiment considering the major differences between the experiments as to projectile mass, beam energy, and the methods used to measure and analyze the low-energy fragment spectra. The fact that $\beta_{\parallel}$ remains small and nearly constant, irrespective of projectile, even for interactions initiated by projectiles with as many as $A = 40$ nucleons in central collisions with target nuclei comparable in mass, is a striking feature of the nucleus-nucleus and p-nucleus interaction.

On a more detailed examination of the angular distributions for fragments $E_p \leq 31$ MeV (Fig. 7 and Table III), systematic deviations from that expected for a Maxwellian distribution characterized by a unique velocity parameter χ_0 are observed. The measured angular spectra consistently show, irrespective of projectile, a nearly isotropic distribution in the forward hemisphere in the laboratory frame, i.e., $\chi_0(0 \leq \mu \leq 1) \approx 0$, whereas the angular distribution in the backward hemisphere is distinctly anisotropic, having angular distribution parameters $\chi_0(-1 \leq \mu \leq 0) \approx 0.3$. Similar behavior in the angular distribution of fragments with ranges $R \leq 3\,mm$ ($\epsilon = 26.4$ MeV/A) emitted from 2.1 GeV/A ^{14}N interactions in emulsions, selected without discrimination, may have been observed by Chernov *et al.*[14] We have fitted their spectrum of $dN/d\cos\theta$ for *black* tracks (taken from their Fig. 2) for the backward and forward hemispheres, as in the present experiment, and have found that the values of χ_0 are, respectively, 0.13 ± 0.11 and 0.04 ± 0.10. Although the statistical uncertainties in these parameters are large, the values themselves are consistent with those obtained in the present experiment, indicating that isotropy in the angular distribution for low-energy fragments emitted in the forward hemisphere is not significantly altered by the inclusion of CNO and peripheral interactions in the measurements. The angular distribution of all fragments emitted from the ^{14}N interactions, with $g \geq 1.4\, g_{\min}$ (equivalent to $E_p \lesssim 500$ MeV), given by Chernov *et al.* are fitted well over all angles [by Eq. (11)] with $\chi_0 = 0.36 \pm 0.02$. This value, when compared to our ^{16}O result of $\chi_0 = 0.26 \pm 0.02$, shows the angular spectra observed by Chernov *et al.* to be more anisotropic, owing to the increase in the upper limit in the fragment energy (i.e., E_p from 250 to 500 MeV) and the inclusion of noncentral collisions as well as CNO interactions in their data sample, all effects that would tend to give increased fragment production in the forward hemisphere.

Jakobsson and Kullberg have examined the energy and angular distributions of protons and He nuclei produced in interaction of 2-GeV/A ^{16}O with emulsion nuclei, the latter classified as to light (CNO) and heavy (AgBr) target nuclei.[13] Interactions in which at least eight units of charge were emitted from the target nucleus were identified as interactions between the ^{16}O projectile and AgBr. By comparing the particle emission for all Ag(Br) interactions to those where the Ag(Br) target nuclei was totally disintegrated, i.e., $n_h \geq 28$, Jakobsson and Kullberg effectively examined AgBr collisions averaged over all impact parameters to those with small impact parameters. They found that the angular distribution of protons $40 < E \lesssim 500$ MeV emitted from $n_h \geq 28$ events, hence, from interactions with small impact parameters, deviates significantly from the angular distribution of protons emitted from the average Ag(Br) collision. Whereas $dN/d\cos\theta$ for protons decreased approximately exponentially for all Ag(Br) events, Jakobsson and Kullberg found that the $n_h \geq 28$, central-collision events yielded an angular spectrum of protons that is deficient of protons at small angles, with $dN/d\cos\theta$ decreasing only slightly between angles of emission 20–120°. They also observed that the $dN/d\cos\theta$ distributions for He nuclei emitted from the $n_h \geq 28$ Ag(Br) events are (i) consistent with isotropy for $E_{\mathrm{He}} \lesssim 10$ MeV/A and (ii) for $10 < E_{\mathrm{He}} < 250$ MeV/A, consistent with isotropy in the forward hemisphere, decreasing with angles between 90–180°. The features of these angular distributions for protons and He nuclei observed by Jakobsson and Kullberg for the high multiplicity events thus exhibit angular distributions similar to those for (unidentified) fragments emitted from selected nonperipheral AgBr events shown in Figs. 4, 7, and 8.

VI. CONCLUSIONS

Although we have discussed how our measured angular spectra differ (an excess of fragments

near 90°) from the assumed Maxwellian distribution we have used for purposes of parametrization and intercomparison of the data, these differences are smooth, well-behaved, and devoid of statistically significant structure.

We summarize the specific conclusions of this emulsion experiment on central collisions between nuclei at 2 GeV/A:

For low energy fragments $E \lesssim 31$ MeV/A:

(1) The angular and range distributions do not depend on the mass of the projectile.

(2) The longitudinal velocities of the emitting systems $\beta_\parallel$ are small, in the range $0.01 < \beta_\parallel < 0.03$ for all projectiles (Table II).

(3) Both $\beta_\parallel$ and β_0 tend to increase with fragment range (energy), but their ratio $\chi_0 = \beta_\parallel/\beta_0$ appears to remain constant.

(4) By invoking the results of Ref. 14, there is no evidence that the angular distribution, hence, $\chi_0 = \beta_\parallel/\beta_0$, depends on the impact parameter of the collision.

(5) The angular distributions are consistent with isotropy in the forward hemisphere, corresponding to $\chi_0 \approx 0$, with $\chi_0 \approx 0.3$ being appropriate for the distribution in the backward hemisphere.

(6) The temperature $\tau = M_n\beta_0^2/2$ is typically 6–7 MeV/A, independent of projectile.

(7) The $dN/d\theta$ distributions are broad, Maxwellian-like, with maxima between 70–75°.

For all fragments with $E \lesssim 250$ MeV/A:

(1) The angular distributions depend on the projectile mass, characterized by values the parameter $\chi_0 \equiv \beta_\parallel/\beta_0 \approx 0.3$ for ^{4}He and ^{16}O beams, and 0.5 for ^{40}Ar.

(2) The $dN/d\theta$ distributions are Maxwellian, with maxima between 55–60°. The angular distributions thus shift toward smaller angles as the energy of the fragment increases.

(3) The number of fragments per event that are emitted in the backward hemisphere depends little on projectile mass, e.g., 6.8, 6.7, and 7.1 for ^{4}He, ^{16}O, and ^{40}Ar, respectively.

Finally, we obtain no evidence in this experiment for structure in either the range or angular distributions of fragments emitted from central collisions between 2 GeV/n ^{4}He, ^{16}O, and ^{40}Ar projectiles and heavy emulsion nuclei. We find there is no unique Maxwellian distribution that successfully describes both the angular and momentum distributions of the observed fragments, hence, no unique particle-emitting system characterized by a longitudinal velocity $\beta_\parallel$ and spectral velocity $\beta_0 = (2\tau/M_n)^{1/2}$.

ACKNOWLEDGMENTS

We thank Margret Banks, Hester Yee, and Robert Turner for their assistance in scanning the nuclear emulsions. We also appreciate the guidance and advice given us by Dr. T. F. Hoang in the analysis and interpretation of the data. We wish to acknowledge R. T. Hagstrom for his critical comments on this paper. This work was carried out under the auspices of U. S. Energy Research and Development Administration, Contract No. W-7405-ENG-48 and the National Aeronautics and Space Administration, Grant No. NGR-05-003-513.

[1] T. D. Lee and G. C. Wick, Phys. Rev. D 9, 2291 (1974).
[2] A. A. Amsden, F. H. Harlow, and J. R. Nix, Phys. Rev. C 15, 2059 (1977).
[3] W. Scheid, H. Muller, and W. Greiner, Phys. Rev. Lett. 32, 741 (1974).
[4] R. K. Smith and M. Danos, in Proceedings of the Meeting on Heavy Ion Collisions, Falls Creek Falls, Tennessee, June 13-17, 1977 (Oak Ridge National Laboratory Report No. CONF-770602), p. 309.
[5] J. P. Bondorf, P. J. Siemens, S. Garpman, and E. C. Halbert, Z. Phys. 279, 385 (1976).
[6] A. R. Bodmer and C. N. Panos, Phys. Rev. C 15, 1342 (1977).
[7] L. Wilets, E. M. Henley, M. Kraft, and A. D. MacKellar, Nucl. Phys. A282, 341 (1977).
[8] J. Hofmann, H. Stocker, U. Heinz, W. Scheid, and W. Greiner, Phys. Rev. Lett. 36, 88 (1976).
[9] H. G. Baumgardt, J. U. Schott, Y. Sakamoto, E. Schopper, H. Stocker, J. Hofmann, W. Scheid, and W. Greiner, Z. Phys. A273, 359 (1975).
[10] J. Gosset, H. H. Gutbrod, W. G. Meyer, A. M. Poskanzer, A. Sandoval, R. Stock, and G. D. Westfall, Phys. Rev. C 16, 629 (1977).
[11] G. D. Westfall, J. Gosset, P. J. Johansen, A. M. Poskanzer, W. G. Meyer, H. H. Gutbrod, A. Sandoval, and R. Stock, Phys. Rev. Lett. 37, 1202 (1976).
[12] B. Jakobsson, R. Kullberg, and I. Otterlund, Nucl. Phys. A276, 523 (1977).
[13] B. Jakobsson and R. Kullberg, University of Lund, Report No. LUIP-CR-75-14, 1975 (unpublished).
[14] G. M. Chernov, K. G. Gulamov, U. G. Gulyamov, S. Z. Nasyrov, and L. N. Svechnikova, Nucl. Phys. A280, 478 (1977).
[15] H. H. Heckman, D. E. Greiner, P. J. Lindstrom, and H. Shwe, Lawrence Berkeley Laboratory Report No. LBL-3656, 1977; Also Phys. Rev. C (to be published).
[16] D. E. Greiner, P. J. Lindstrom, H. H. Heckman, Bruce Cork, and F. S. Bieser, Phys. Rev. Lett. 35, 152 (1975).
[17] R. Kullberg, I. Otterlund, and R. Resman, Phys. Scr. 5, 5 (1972).
[18] P. Ciok, T. Saniewska, P. Zielinski, D. Haskin, and E. Lohrmann, Nucl. Phys. 40, 260 (1963).
[19] J. D. Sullivan, P. B. Price, H. J. Crawford, and M. Whitehead, Phys. Rev. Lett. 30, 126 (1973).
[20] F. James and M. Roos, Lawrence Berkeley Labora-

tory version of program MINUIT, CERN Computer Center, August, 1975 (unpublished).
[21]J. M. Alexander, in *Nuclear Chemistry*, edited by L. Yaffe (Academic, New York, 1968), Vol. I, p. 273.
[22]E. K. Hyde, G. W. Butler, and A. M. Poskanzer, Phys. Rev. C 4, 1759 (1971).
[23]A. S. Goldhaber, Phys. Lett. 53B, 306 (1974).
[24]B. Andersson, I. Otterlund, and K. Kristiansson, Ark. Fys. 31, 527 (1966).
[25]B. Jakobsson, R. Kullberg, and I. Otterlund, Nucl. Phys. A276, 523 (1977).
[26]M. Bogdanski, E. Jeannet, and C. Metzgen, Helv. Phys. Acta. 42, 485 (1969).
[27]E. W. Baker, S. Katcoff, and C. P. Baker, Phys. Rev. 117, 1352 (1960).
[28]J. Bogdanowicz, P. Ciok, Z. Galster, T. Saniewska, and P. Zielinski, Nucl. Phys. 40, 260 (1963).
[29]O. Skaggestad and S. O. C. Sorensen, Phys. Rev. 113, 1115 (1959).
[30]W. Gajewski, J. Pniewski, J. Sieminska, J. Suchorzweska, and P. Zielinski, Nucl. Phys. 58, 17 (1964).
[31]N. P. Bogachev, E. L. Grigoriev, Yu. P. Merekov, and N. A. Nitkin, Zh. Eksp. Teor. Fiz. 44, 493 (1963) [Sov. Phys.-JETP 17, 337 (1963)].
[32]N. P. Bogachev, A. G. Volod'ko, E. L. Grigorev, and Yu. P. Merelov, Zh. Eksp. Teor. Fiz. 44, 1869 (1963) [Sov. Phys.-JETP 17, 1257 (1963)].
[33]R. Stein, Nucl. Phys. 87, 854 (1967).